A salt-rejecting solar evaporator for continuous steam generation

Xiao, Yangyi; Wang, Xun; Li, Chenxing; Peng, Huan; Zhang, Tuqiao; Ye, Miaomiao

DOI
10.1016/j.jece.2020.105010

Publication date
2021

Document Version
Final published version

Published in
Journal of Environmental Chemical Engineering

Journal of Environmental Chemical Engineering 9 (2021) 105010

Contents lists available at ScienceDirect

Journal of Environmental Chemical Engineering

journal homepage: www.elsevier.com/locate/jece

A salt-rejecting solar evaporator for continuous steam generation

Yangyi Xiao [a], Xun Wang [a,b], Chenxing Li [a], Huan Peng [a], Tuqiao Zhang [a], Miaomiao Ye [a,*]

[a] Zhejiang Key Laboratory of Drinking Water Safety and Distribution Technology, College of Civil Engineering and Architecture, Zhejiang University, Hangzhou 310058, PR China

[b] Section of Sanitary Engineering, Department of Water Management, Faculty of Civil Engineering and Geosciences, Delft University of Technology, P.O. Box 5048, 2600 GA Delft, Netherlands

ARTICLE INFO

Editor: Dr. Zhang Xiwang

Keywords:
Solar desalination
Solar evaporator
Interfacial solar heating
Salt-rejecting

ABSTRACT

Recently, great efforts have been focused on solar evaporators because they can localize solar heat on the air-water interface resulting in enhanced photothermal conversion efficiency. However, to prevent salt accumulation during evaporation while maintaining high evaporation rates is still a challenge. In this work, a salt-rejecting solar evaporator was fabricated for continuous seawater desalination. The evaporator was composed of a top layer of carbon black (CB) nanoparticles for solar absorbance, an interlayer of superhydrophilic melamine formaldehyde (MF) foam for both seawater and concentrated brine delivery, and an outlayer of expandable polyethylene (EPE) foam for floating and heat insulation. The superhydrophilic MF foam could offer a channel for rapid exchange of the concentrated brine with the solution beneath, thereby preventing salt accumulation in the evaporator. It was demonstrated that the salt-rejecting solar evaporator produced a high water evaporation rate of 1.24 $kg{\cdot}m^{-2}{\cdot}h^{-1}$ under 1 $kW{\cdot}m^{-2}$ solar irradiance, which was 3.2 times higher than that of the pristine simulated seawater (3.5 wt% NaCl solution). Furthermore, the salt-rejecting evaporator displayed an excellent stability as the water evaporation rate remained constant even after 16-cycles of use within 20 days.

1. Introduction

Fresh water scarcity, caused by the climate change, population growth, socio-economic and industrialization, has become a massive crisis that urgently needs to be solved [1–3]. Seawater desalination has been denoted as the most suitable solution to get rid of this issue, because it can offer an unlimited and steady supply of high-quality water without impairing natural freshwater ecosystems [4–6]. Currently, the major desalination technologies are thermal distillation (e.g. multi-stage flash) and membrane separation (e.g. reverse osmosis). However, both of these two types of desalinations are infeasible for large-scale use in remote and impoverished areas due to their high energy consumption, complex processes, and high cost [7–9].

Recently, a new concept named "air-water interfacial solar heating" has been proposed for seawater desalination [10,11]. It has attracted much attention due to its low energy consumption, high water evaporation rate, low cost, and simple operation [12–14]. In this approach, photothermal materials float on the water surface and rapidly heat the air-water interface, avoiding heating the bulk water, thus it is a more efficient approach compared with traditional thermal distillation approaches [15,16]. However, the evaporation rates of the floating photothermal materials are not high (usually in the range of 0.5–1.0 $kg{\cdot}m^{-2}{\cdot}h^{-1}$) due to the heat loss to the bulk solution beneath [17–21]. In order to reduce heat loss, thus improving the water evaporation rate, photothermal materials were combined with thermal insulation materials and/or water-absorbing materials to form solar evaporators. The water evaporation rate of the as-designed evaporators can be significantly enhanced to >1.2 $kg{\cdot}m^{-2}{\cdot}h^{-1}$ under 1 sun irradiance [22–26]. However, salt may accumulate in the evaporators and block the channels for vapor escape during desalination process which results in the decrease of fresh water yield and sometimes destruction of the evaporators [27–30]. Therefore, salt accumulation in the evaporators under continuous operation needs to be addressed.

In this work, a salt-rejecting solar evaporator was fabricated for continuous seawater desalination based on the new concept of "air-water interfacial solar heating". In this evaporator, commercial carbon black (CB) nanoparticles were used as the photothermal material for solar absorption because of their high absorbance, excellent mechanical strength, and low cost [31]. Superhydrophilic melamine formaldehyde (MF) foam was used as a water delivery channel for rapid exchange of the concentrated brine with the beneath solution due to its superhydrophilicity, strong durability, and low cost [32]. Expandable

* Corresponding author.
E-mail address: yemiao008@zju.edu.cn (M. Ye).

https://doi.org/10.1016/j.jece.2020.105010
Received 19 October 2020; Received in revised form 3 December 2020; Accepted 28 December 2020
Available online 31 December 2020

polyethylene (EPE) foam was used as both the support of the MF and the peripheral thermal insulation material due to its low density and high specific heat capacity [33]. Therefore, a solar evaporator with stable high evaporation rate, simple structure, salt-rejecting property, and low-cost was obtained. The concentrated brine, which was formed during the solar desalination process, could be rapidly exchanged with the solution beneath. As a result, the salt-rejecting evaporator enabled real-time concentrated brine discharge during continuous solar desalination even in 14.0 wt% NaCl solution.

2. Materials and methods

2.1. Chemicals

All chemicals were of an analytical grade and used as received without any further purification. Sodium chloride (NaCl) was purchased from the Sinopharm Chemical Reagent Company. Copper sulfate pentahydrate ($CuSO_4{\cdot}5H_2O$) was purchased from the Sinopharm Chemical Reagent Company. Carbon black nanoparticles (CB, 99.5%, 30 nm) were purchased from the Shanghai Aladdin Industrial Co., China. Carbon nanotubes (CNTs assay: 70%−80% (Carbon content, TGA)) were purchased from the Sigma−Aldrich, USA. MoS_2 nanoflowers were prepared by a simple hydrothermal process which has been reported in our previous work [34]. Air-laid cloth (ALC) and air-laid paper (ALP) were purchased from the Suzhou Baichen Co., China. Expandable polyethylene (EPE density: 12.2 kg/m^3) foams were purchased from the Shunyibaocai Co., China. Melamine formaldehyde (MF density: 8.7 kg/m^3) foams were obtained from the Zhejiang LeDian Co., China. Polyurethane (PU) foams (PU density: 15 kg/m^3) were purchased from the Lianyahaimian Co., China.

2.2. Preparation of salt-rejecting solar evaporator

First, a certain amount of CB nanoparticles was dispersed in 30 mL ultrapure water with ultrasonication for 30 min to form a black suspension, then a piece of ALC with a diameter of 4 cm was immersed into the black suspension for 60 min with ultrasonication to form the ALC/CB absorbance layer. Second, an EPE foam cylindrical ring with an outer diameter of 6 cm and an inner diameter of 4 cm was cut out to form an insulation layer for both supporting the MF foam and peripheral thermal isolation (Fig. S1a, Supporting Information). Third, a piece of white cylindrical MF foam with a diameter of 4 cm, as a delivery channel for exchange between concentrated brine and seawater, was embedded in the EPE foam cylindrical ring (Fig. S1b, Supporting Information). Finally, the salt-rejecting solar evaporator was obtained by placing the ALC/CB absorbance layer on the MF foam (Fig. S1c, Supporting Information). In order to further demonstrate the salt-rejection process, other evaporators as control samples with the same structure but different photothermal materials such as CNTs and MoS_2 and different interlayer foam such as PU foam were constructed with the same process above.

2.3. Water evaporation experiment

The water evaporation experiments were conducted at a temperature of 22 °C ± 1 °C and humidity of 50% ± 10% to evaluate the solar evaporation rate and salt-rejection properties of the solar evaporator. The salt-rejecting solar evaporator was placed in a 250 mL beaker with 200 mL of 3.5 wt% NaCl solution under the irradiance of a xenon lamp (XES−40S3 −TT, SAN−EI ELECTRIC Japan). The evaporated mass of the 3.5 wt% NaCl solution during the whole evaporation process was measured by an electronic balance (MP1100B, Shanghai Shun Yuheng Scientific Instruments Co., China).

2.4. Characterization

The microstructure of MF foam was observed by a field emission scanning electron microscope (SEM, FEI, Quanta FEG 650) at an acceleration of 15 kV. The temperature condition of the salt-rejecting solar evaporator's surface was monitored by a thermal infrared imager (S65, FLIR). The contact angle of MF foam was observed by a video contact angle measuring instrument (DATAPHYSI, OCA20). The surface functional groups of the MF were analyzed with the Fourier transform infrared spectrometer (FTIR, Nicolet, iS50).

3. Results and discussion

3.1. Characterization of the salt-rejecting evaporator

The salt-rejecting property of the evaporator was realized through the rapid exchange between the concentrated brine and the underlying solution in the superhydrophilic MF foam. Therefore, the superhydrophilicity of the MF foam was first confirmed by the FTIR spectrum (Fig. 1a). The transmission peak at 3324 cm^{-1} was ascribed to the stretching vibration of –NH− and −OH groups and the peak at 1686 cm^{-1} was caused by the stretching vibration of C=O in carbonyl group. Meanwhile, those peaks at 1541, 1456, 1328 and 810 cm^{-1} could be identified as the characteristics of triazine ring. The transmission peak at 981 cm^{-1} was designated to the stretching vibration of C−O and N–H. All the functional groups endowed the MF foam a hydrophilic surface [35,36]. Second, the MF foam had a reticulated structure where struts are responsible for the main inner area, and the size of holes ranges from tens to hundreds of microns so that the MF foam had an excellent water absorption capacity (Fig. 1b). Third, the contact angle of the MF foam was observed to further confirm its superhydrophilicity. As shown in Fig. 1c, a water drop was absorbed within 0.078 s and the water contact angle dropped to 0° rapidly, suggesting the superhydrophilicity of the MF foam. Fourth, the water-uptake behavior of the MF foam was also monitored to evaluate its wettability property. The water absorption rate was tested by means of placing EPE/MF in methylene blue solution to visualize liquid movement. The MF foam could be fully saturated and wetted within 1.5 s (Fig. S2, Supporting Information) and the calculated water absorption rate was 3.1×10^4 kg m$^{-2}{\cdot}$h^{-1}, which ensures adequate water for concentrated brine exchange in MF foam.

3.2. Water evaporation and salt-rejection

The water evaporation performance of the salt-rejecting solar evaporator was calculated by measuring the evaporated water mass. In comparison, the water evaporation experiments of simulated seawater (3.5 wt% NaCl solution) alone and the salt-rejecting solar evaporator without CB deposition were carried out. As presented in Fig. 2a, all of the solar evaporation processes can be simply modeled by the zero-order kinetics and described by Eq. (1).

$$m - m_0 = -kt \quad (1)$$

where m and m_0 are the actual water mass at time t and the initial water mass, respectively, and k represents the water evaporation rate. The water evaporation rate of the salt-rejecting solar evaporator was 1.24 kg·m$^{-2}{\cdot}$h^{-1} under 1 kW·m^{-2} solar irradiance, which was 1.5 times and 3.2 times higher than the salt-rejecting solar evaporator without CB deposition and the pristine simulated seawater respectively. No salt accumulation was found on the surface of the salt-rejecting evaporator while there was obvious salt accumulation on the surface of the salt-accumulation evaporator (inset in Fig. 2b), indicating that the MF foam was the main site for the exchange between the concentrated brine and the underlying NaCl solution. In addition, the photothermal conversion efficiency (η) could also be calculated by using Eq. (2).

$$\eta = mh_{LV}/C_{OPT}P_0 \quad (2)$$

where h_{LV} is the total enthalpy of liquid-vapor phase change, m is the evaporation rate (kg·m$^{-2}{\cdot}$h^{-1}), C_{OPT} is optical concentration and P_0 is

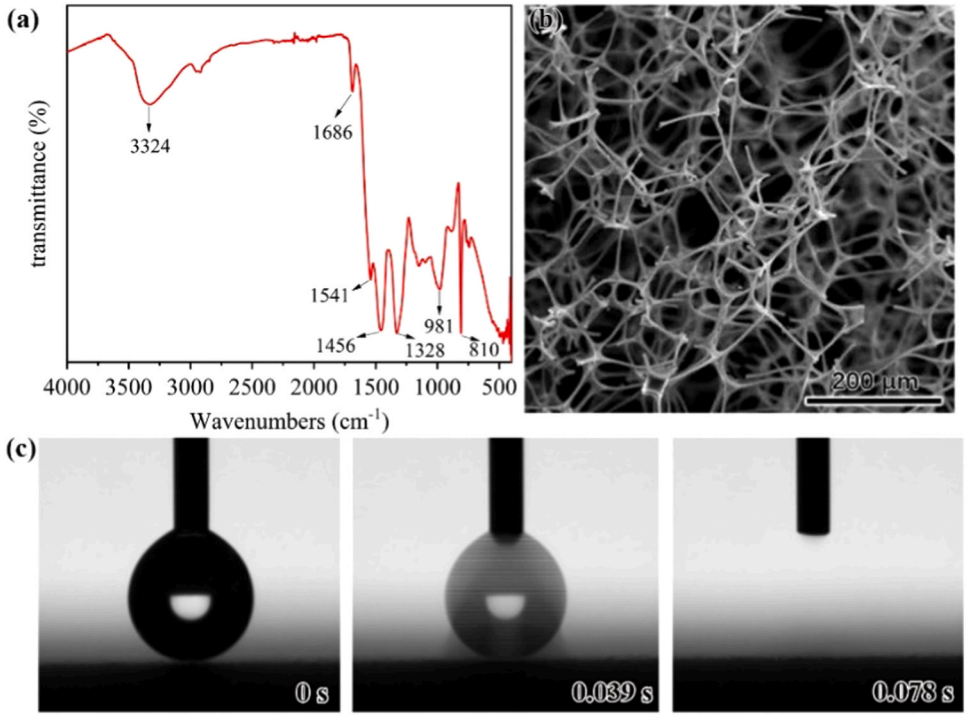

Fig. 1. (a) SEM, (b) FT−IR spectrum, and (c) contact angle of the MF foam.

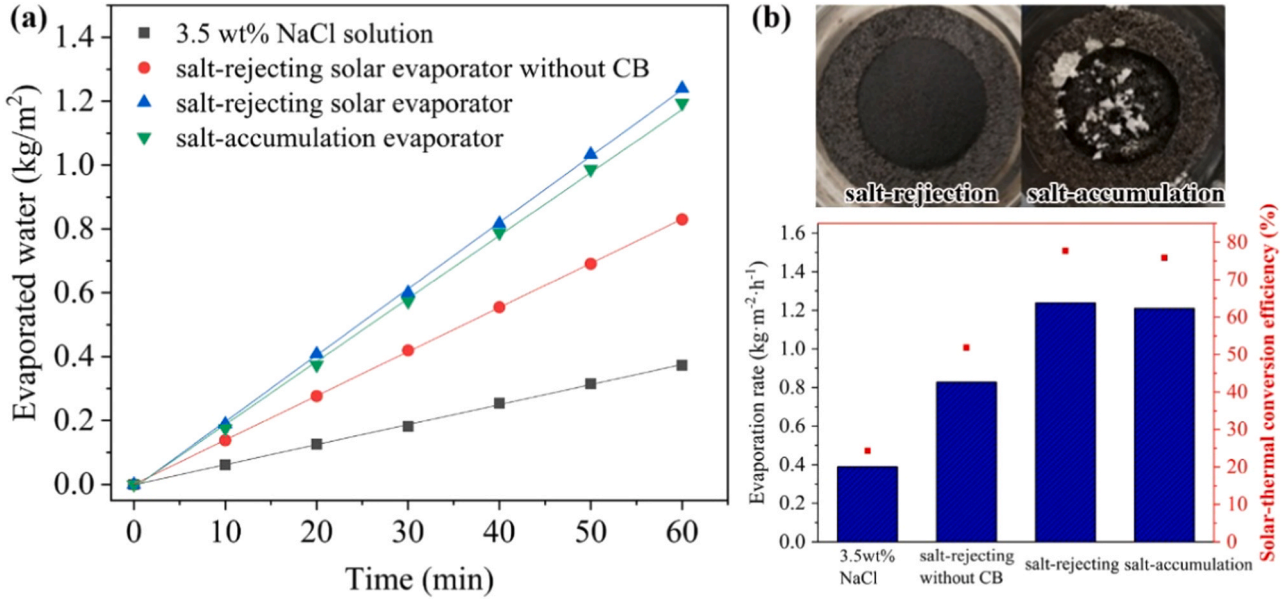

Fig. 2. (a) Evaporated water mass as a function of irradiation time in the evaporation processes of the simulated seawater (3.5 wt% NaCl solution) and different solar evaporators. (b) Water evaporation rate, photothermal conversion efficiency, and surface salt-accumulation appearance of different solar evaporators after 4 h light irradiation in simulated seawater (3.5 wt% NaCl solution).

the nominal direct solar irradiation 1 kW·m^{-2}. As calculated, the η of the salt-rejecting evaporator was 77.8%, which was higher than the pristine simulated seawater. This result proved that the salt-rejecting evaporator can enable effective interfacial solar heating.

The interfacial solar heating effect was further proved by testing the surface temperature change of the salt-rejecting solar evaporator during the evaporation process. As shown in Fig. S3a and d, Supporting Information, the air-water interface temperatures with and without the salt-rejecting solar evaporator were 14.0 °C and 15.6 °C respectively before 1 kW·m^{-2} solar irradiance. After irradiance for 60 min, the air-water interface temperature of the salt-rejecting solar evaporator increased to 34.5 °C while the control group was 22.6 °C, which indicates that EPE/MF layer could prevent heat transfer to the bulk water.

To explore water evaporation efficiency and salt-rejection characteristic of the evaporator, water evaporation experiments were conducted under different NaCl concentrations. The water evaporation rate slightly decreased from 1.24 to 1.15 kg·m^{-2}·h^{-1} (accompanied by the decrease of the photothermal conversion efficiency from 77.8% to 72.2%, as shown in Fig. 3b) with the concentrations of the NaCl solution increased from 3.5 to 14 wt%, which was probably due to the principle

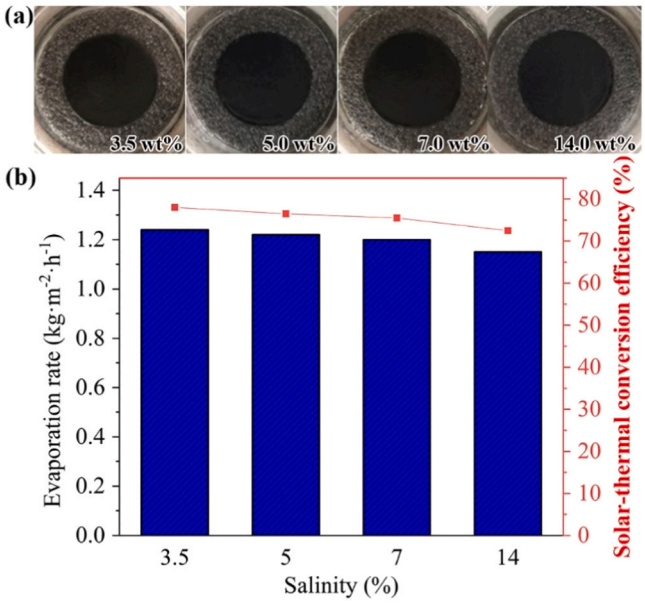

Fig. 3. (a) Digital photos and (b) water evaporation rate and photothermal conversion efficiency of the salt-rejecting solar evaporator after 4 h light irradiation under different NaCl concentrations.

that the vapor pressure of water decreases with the increased salinity [37]. However, because of the rapid exchange between the concentrated brine and the underlying NaCl solution, no salt accumulation occurred on the surface of the evaporator, even under the high NaCl concentration of 14 wt% (Fig. 3a), indicating its excellent salt-rejecting property. To further explore the salt-rejection behavior, a solar evaporation experiment was conducted with $CuSO_4{\cdot}5H_2O$ particles on the surface of the evaporator (Fig. 4a). It can be seen that the mass of $CuSO_4{\cdot}5H_2O$ gradually decreased with the evaporation time. The 8 g of $CuSO_4{\cdot}5H_2O$ completely dissolved into the underlying solution, which caused the transparent solution to turn blue after 4 h solar irradiation (Fig. 4b). This phenomenon strongly suggests that the salt-rejection could be realized by transporting the concentrated brine back into the underlying solution as long as the concentration of the brine was below the salt's saturation concentration.

The effects of CB nanoparticles dose, MF foam thickness, solar intensity and relative humidity on the water evaporation rate, photothermal conversion efficiency and salt-rejection characteristic of the salt-rejecting solar evaporator were studied to optimize the operation conditions, and the results are shown in Fig. S4, Supporting Information. The water evaporation rate increased from 1.04 to 1.16 kg m^{-2} h^{-1} (accompanied by the η values increased from 65.3% to 72.8%) with the CB nanoparticles dose increasing from 5 to 15 mg and almost remained unchanged when further increasing CB dose from 15 to 25 mg (Fig. 5a). The water evaporation rate and photothermal conversion efficiency significantly increased with the growth of MF foam thickness until the thickness achieved 1.5 cm (Fig. 5b) which illustrates the excellent insulation property of MF foam. As optimized, the CB nanoparticles dose of 15 mg and MF thickness of 1.5 cm were used in the following evaporation experiments. Moreover, the water evaporation rate of 1.24 $kg{\cdot}m^{-2}{\cdot}h^{-1}$ with the calculated photothermal conversion efficiency of 77.8% was obtained under the optimal conditions previously described. The water evaporation efficiency of the as-prepared salt-rejecting evaporator was higher than a variety of the reported efficiencies of other salt-rejecting evaporators (Table S1). The water evaporation rate was significantly enhanced with increased solar intensity (Fig. 5c). However, as the temperature at the gas-liquid interface increased with the solar intensity, more heat was lost due to the heat radiation. Accordingly, the photothermal conversion efficiency decreased from 79.2% to 72.0%. The effect of the relative humidity on the water evaporation rate was carried out by setting the relative humidity at 55%, 70% and 90% while keeping other operation conditions unchanged. As shown in Fig. 5d, the water evaporation rate slightly decreased from 1.24 $kg{\cdot}m^{-2}{\cdot}h^{-1}$ to 1.20 $kg{\cdot}m^{-2}{\cdot}h^{-1}$ when the relative humidity increased from 55% to 70%. Moreover, the solar evaporation was still able to maintain at a high rate of 1.10 $kg{\cdot}m^{-2}{\cdot}h^{-1}$ even when the relative humidity greatly increased to 90%. Importantly, no salt accumulation (except in the case of the thinner MF foam, in which a little water could diffuse into the top of EPE foam from between EPE foam and beaker due to the tension of the water) on the surface of the evaporator occurred (Figs. S5 and S6, Supporting Information) when optimizing the operation conditions, indicating the excellent salt-rejection property of the evaporator.

To further demonstrate that the salt-rejecting property of the evaporator was realized through the rapid exchange between the concentrated brine and the underlying solution in the MF foam, another two solar evaporators with the same structure but different photothermal materials, CNTs and MoS_2, were fabricated. As shown in Fig. 6a-c, the change of photothermal materials had no effect on the salt-rejecting property of the evaporators except that the water evaporation rate decreased from 1.24 to 1.14 $kg{\cdot}m^{-2}{\cdot}h^{-1}$ with the corresponding photothermal conversion efficiency decreased from 77.8% to 71.6% (Fig. 6d). The slightly reduced k and η values were mainly due to the lower relative solar absorbance of the CNTs and MoS_2.

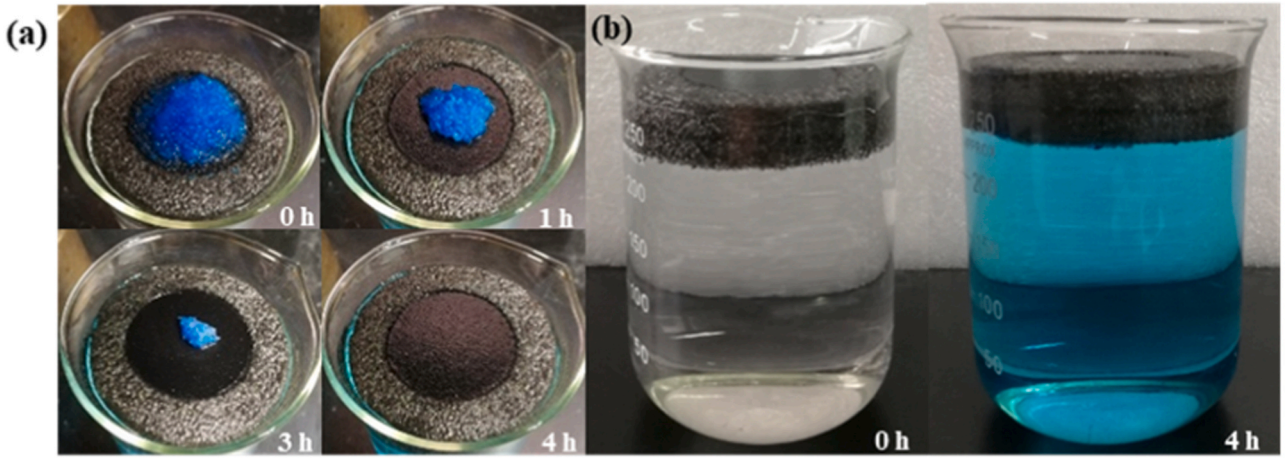

Fig. 4. (a) Top and (b) front view of the dissolution behavior of the $CuSO_4{\cdot}5H_2O$ particles in the evaporation processing using the salt-rejecting solar evaporator.

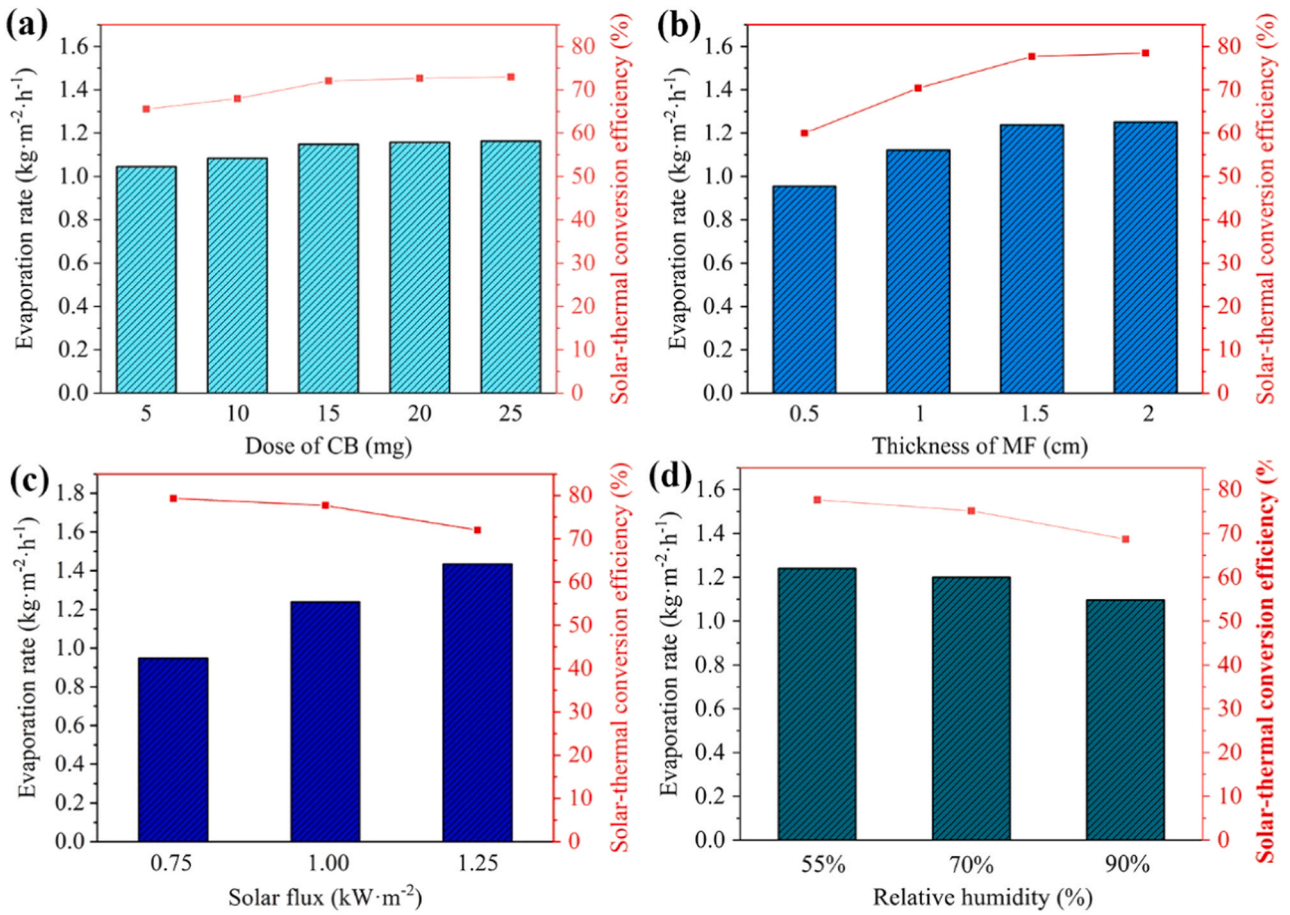

Fig. 5. The effects of (a) CB nanoparticles dose, (b) MF thickness (c) solar intensity and (d) relative humidity on water evaporation rate and photothermal conversion efficiency of the salt-rejecting solar evaporator.

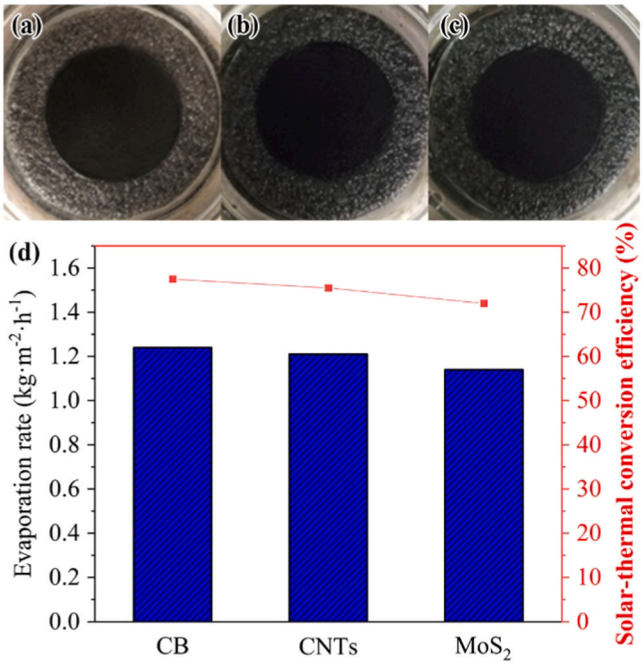

Fig. 6. Digital photos of the salt-rejecting solar evaporators with different photothermal materials of (a) CB nanoparticles (b) CNTs and (c) MoS_2 after 4 h irradiation; (d) The water evaporation rate and photothermal conversion efficiency of different photothermal materials.

3.3. Stability and durability

Stability and durability are important properties because they determine the service life of salt-rejecting evaporator which influences the cost of the fresh water in the next step. Here, real seawater obtained from the East China Sea was used for investigating the stability and durability of the salt-rejecting evaporator during 16 cycles of use. As shown in Fig. 7a, the surface of the evaporator operated without salt accumulation in repeated cycles of use which confirms the excellent salt-rejecting property of the as-prepared solar evaporator. Furthermore, the water evaporation rate and the conversion efficiency also remained unchanged (Fig. 7b) over the whole measured period suggesting good stability and durability of the salt-rejecting evaporator.

To explore the potential application of the salt-rejecting evaporator in practical settings of solar desalination, a scaled-up salt-rejecting evaporator with the dimension of 12 cm × 12 cm × 1.5 cm (length × width × height respectively) was fabricated (Fig. 8a). The solar evaporation experiments were carried out outdoor at the Beijing time from 9:00 am to 15:00 pm. After 6 h of natural solar irradiance, the 144 cm^2 surface of the scaled-up evaporator remained intact without salt accumulation, indicating the excellent salt-rejecting property of the scaled-up evaporator. The water evaporation rates at each 1 h interval were calculated (Fig. 8b), and the average evaporation rate was 0.78 $kg{\cdot}m^{-2}{\cdot}h^{-1}$ with the highest value of 0.82 $kg{\cdot}m^{-2}{\cdot}h^{-1}$ and lowest value of 0.73 $kg{\cdot}m^{-2}{\cdot}h^{-1}$. Correspondingly, the photothermal conversion efficiencies under different time intervals were maintained in the range of 68.3% to 72.3%, indicating the high photothermal conversion efficiency and stability of the scaled-up salt-rejecting evaporator.

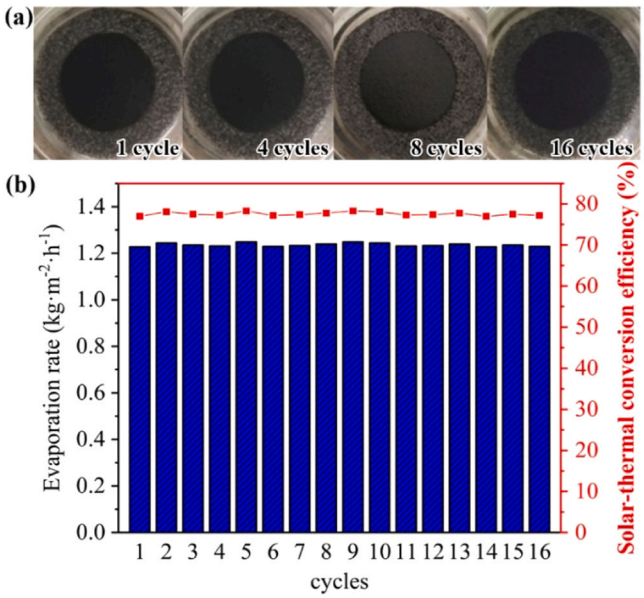

Fig. 7. (a) Digital photos and (b) water evaporation rate and photothermal conversion efficiency of the salt-rejecting solar evaporator under 1 sun solar irradiance during 16 cycles of use.

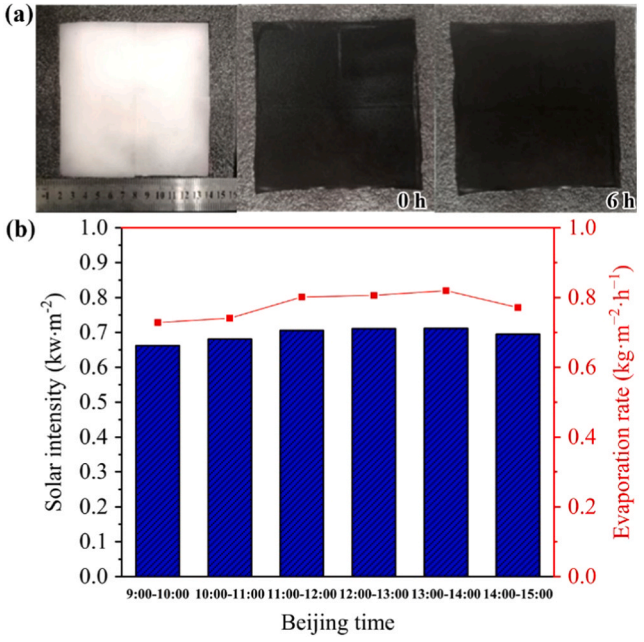

Fig. 8. (a) Digital photos of the scaled-up salt-rejecting solar evaporator before and after 6 h' solar evaporation. (b) Solar intensity and photothermal conversion efficiency at different time period in outdoor evaporation experiments.

4. Conclusion

In summary, a salt-rejecting solar evaporator was fabricated for continuous solar steam generation based on the new concept of "air-water interfacial solar heating". The salt-rejecting property of the evaporator was realized through rapid exchange between concentrated brine and the solution beneath using superhydrophilic MF foam. As a result, the salt-rejecting evaporator enabled real-time concentrated brine discharge during continuous solar desalination even in high salinity seawater. The water evaporation rate of the salt-rejecting solar evaporator was 1.24 $kg \cdot m^{-2} \cdot h^{-1}$ (accompanied by a photothermal conversion efficiency of 77.8%) under 1 $kW \cdot m^{-2}$ solar irradiance. The salt-rejecting evaporator also displayed good durability as the evaporation rate was almost unchanged even after 16 cycles of use. We believe that the high evaporation rate, salt-rejection property, simple structure, scalability, low-cost, as well as the good durability and stability make the as-prepared salt-rejecting evaporator potentially useful in practical settings of solar desalination in island areas.

Supplementary data

The fabrication process of the salt-rejecting evaporator; Water-uptake behavior of the MF foam; Effects of CB dose, MF thickness and solar intensity on water evaporation rate and salt-accumulation characteristic.

CRediT authorship contribution statement

Yangyi Xiao: Investigation, Data curation, Writing - original draft. **Xun Wang:** Investigation, Data curation. **Chenxing Li:** Investigation, Data curation. **Huan Peng:** Formal analysis. **Tuqiao Zhang:** Supervision, Funding acquisition. **Miaomiao Ye:** Conceptualization, Supervision, Writing - review & editing, Project administration.

Declaration of Competing interest

The authors declare that they have no known competing financial interests or personal relationships that could have appeared to influence the work reported in this paper.

Acknowledgements

Yangyi Xiao and Xun Wang contributed equally to this work. The present work was financially supported by the National Natural Science Foundation of China (No. 52070161 and No. 51761145022), the National Science and Technology Major Protects for Water Pollution Control and Treatment (No. 2017ZX07201004), the Public Welfare Technology Application Research Project of Zhejiang Province (No. LGG18E080002).

Appendix A. Supporting information

Supplementary data associated with this article can be found in the online version at doi:10.1016/j.jece.2020.105010.

References

[1] J. Alcamo, M. Floerke, M. Maerker, Future long-term changes in global water resources driven by socio-economic and climatic changes, Hydrol. Sci. J. 52 (2007) 247–275.
[2] M. Kummu, J.H.A. Guillaume, H. de Moel, S. Eisner, M. Floerke, M. Porkka, S. Siebert, T.I.E. Veldkamp, P.J. Ward, The world's road to water scarcity: shortage and stress in the 20th century and pathways towards sustainability, Sci. Rep. 6 (2016) 38495.
[3] M. Elimelech, W.A. Phillip, The future of seawater desalination: energy, technology, and the environment, Science 333 (2011) 712–717.
[4] N. Voutchkov, Energy use for membrane seawater desalination - current status and trends, Desalination 431 (2018) 2–14.
[5] M.A. Shannon, P.W. Bohn, M. Elimelech, J.G. Georgiadis, B.J. Marinas, A. M. Mayes, Science and technology for water purification in the coming decades, Nature 452 (2008) 301–310.
[6] G.H. Liu, J.L. Xu, K.Y. Wang, Solar water evaporation by black photothermal sheets, Nano Energy 41 (2017) 269–284.
[7] Z.T. Li, C.B. Wang, J.B. Su, S. Ling, W. Wang, M. An, Fast-growing field of interfacial solar steam generation: evolutional materials, engineered architectures, and synergistic applications, Sol. RRL 3 (2019), 1800206.
[8] Y. Yang, R. Zhao, T. Zhang, K. Zhao, P. Xiao, Y. Ma, P.M. Ajayan, G. Shi, Y. Chen, Graphene-based standalone solar energy converter for water desalination and purification, ACS Nano 12 (2018) 829–835.
[9] Y. Liu, S. Yu, R. Feng, A. Bernard, Y. Liu, Y. Zhang, H. Duan, W. Shang, P. Tao, C. Song, T. Deng, A bioinspired, reusable, paper-based system for high-performance large-scale evaporation, Adv. Mater. 27 (2015) 2768–2774.

[10] L.B. Zhang, B. Tang, J.B. Wu, R.Y. Li, P. Wang, Hydrophobic light-to-heat conversion membranes with self-healing ability for interfacial solar heating, Adv. Mater. 27 (2015) 4889–4894.
[11] R. Chen, Z.J. Wu, T.Q. Zhang, T.C. Yu, M.M. Ye, Magnetically recyclable self-assembled thin films for highly efficient water evaporation by interfacial solar heating, RSC Adv. 7 (2017) 19849–19855.
[12] G. Ni, G. Li, S.V. Boriskina, H. Li, W. Yang, T. Zhang, G. Chen, Steam generation under one sun enabled by a floating structure with thermal concentration, Nat. Energy 1 (2016) 16126.
[13] H.D. Liu, Z. Huang, K. Liu, X.J. Hu, J. Zhou, Interfacial solar-to-heat conversion for desalination, Adv. Energy Mater. 9 (2019), 1900310.
[14] L.L. Zhu, M.M. Gao, C.K.N. Peh, G.W. Ho, Recent progress in solar-driven interfacial water evaporation: advanced designs and applications, Nano Energy 57 (2019) 507–518.
[15] H. Ghasemi, G. Ni, A.M. Marconnet, J. Loomis, S. Yerci, N. Miljkovic, G. Chen, Solar steam generation by heat localization, Nat. Commun. 5 (2014) 4449.
[16] P. Tao, G. Ni, C.Y. Song, W. Shang, J.B. Wu, J. Zhu, G. Chen, T. Deng, Solar-driven interfacial evaporation, Nat. Energy 3 (2018) 1031–1041.
[17] M.M. Ye, J. Jia, Z.J. Wu, C.X. Qian, R. Chen, P.G. O'Brien, W. Sun, Y.C. Dong, G. A. Ozin, Synthesis of black TiOx nanoparticles by Mg reduction of TiO_2 nanocrystals and their application for solar water evaporation, Adv. Energy Mater. 7 (2017), 1601811.
[18] Y.M. Liu, J.W. Chen, D.W. Guo, M.Y. Cao, L. Jiang, Floatable, self-cleaning, and carbon-black-based superhydrophobic gauze for the solar evaporation enhancement at the air-water interface, ACS Appl. Mater. Interfaces 7 (2015) 13645–13652.
[19] Y. Zeng, J.F. Yao, B.A. Horri, K. Wang, Y.Z. Wu, D. Li, H.T. Wang, Solar evaporation enhancement using floating light-absorbing magnetic particles, Energy Environ. Sci. 4 (2011) 4074–4078.
[20] O. Neumann, A.S. Urban, J. Day, S. Lal, P. Nordlander, N.J. Halas, Solar vapor generation enabled by nanoparticles, ACS Nano 7 (2013) 42–49.
[21] V. Kashyap, A. Al-Bayati, S.M. Sajadi, P. Irajizad, S.H. Wang, H. Ghasemi, A flexible anti-clogging graphite film for scalable solar desalination by heat localization, J. Mater. Chem. A 5 (2017) 15227–15234.
[22] Y. Xu, D. Liu, H. Xiang, S. Ren, Z. Zhu, D. Liu, H. Xu, F. Cui, W. Wang, Easily scaled-up photo-thermal membrane with structure-dependent auto-cleaning feature for high-efficient solar desalination, J. Membr. Sci. 586 (2019) 222–230.
[23] Q. Gan, T. Zhang, R. Chen, X. Wang, M. Ye, Simple, low-dose, durable, and carbon-nanotube-based floating solar still for efficient desalination and purification, ACS Sustain. Chem. Eng. 7 (2019) 3925–3932.
[24] R. Chen, X. Wang, Q. Gan, T. Zhang, K. Zhu, M. Ye, A bifunctional MoS_2-based solar evaporator for both efficient water evaporation and clean freshwater collection, J. Mater. Chem. A 7 (2019) 11177–11185.
[25] H. Kou, Z. Liu, B. Zhu, D.K. Macharia, S. Ahmed, B. Wu, M. Zhu, X. Liu, Z. Chen, Recyclable CNT-coupled cotton fabrics for low-cost and efficient desalination of seawater under sunlight, Desalination 462 (2019) 29–38.
[26] X. Zhou, F. Zhao, Y. Guo, Y. Zhang, G. Yu, A hydrogel-based antifouling solar evaporator for highly efficient water desalination, Energy Environ. Sci. 11 (2018) 1985–1992.
[27] S.M. He, C.J. Chen, Y.D. Kuang, R.Y. Mi, Y. Liu, Y. Pei, W.Q. Kong, W.T. Gan, H. Xie, E. Hitz, C. Jia, X. Chen, A. Gong, J.M. Liao, J. Li, Z.J. Ren, B. Yang, S. Das, L. B. Hu, Nature-inspired salt resistant bimodal porous solar evaporator for efficient and stable water desalination, Energy Environ. Sci. 12 (2019) 1558–1567.
[28] G. Ni, S.H. Zandavi, S.M. Javid, S.V. Boriskina, T.A. Cooper, G. Chen, A salt-rejecting floating solar still for low-cost desalination, Energy Environ. Sci. 11 (2018) 1510–1519.
[29] Y. Shi, C.L. Zhang, R.Y. Li, S.F. Zhuo, Y. Jin, L. Shi, S. Hong, J. Chang, C.S. Ong, P. Wang, Solar evaporator with controlled salt precipitation for zero liquid discharge desalination, Environ. Sci. Technol. 52 (2018) 11822–11830.
[30] Y.D. Kuang, C.J. Chen, S.M. He, E.M. Hitz, Y.L. Wang, W.T. Gan, R.Y. Mi, L.B. Hu, A high-performance self-regenerating solar evaporator for continuous water desalination, Adv. Mater. 31 (2019), 1900498.
[31] A. Zeiny, H.C. Jin, G.P. Lin, P.X. Song, D.S. Wen, Solar evaporation via nanofluids: a comparative study, Renew. Energy 122 (2018) 443–454.
[32] V. Nemanic, B. Zajec, M. Zumer, N. Figar, M. Kavsek, I. Mihelic, Synthesis and characterization of melamine-formaldehyde rigid foams for vacuum thermal insulation, Appl. Energy 114 (2014) 320–326.
[33] X. Wang, M. Gan, R. Chen, H. Peng, T.Q. Zhang, M.M. Ye, Water delivery channel design in solar evaporator for efficient and durable water evaporation with salt rejection, ACS Sustain. Chem. Eng. 8 (2020) 7753–7761.
[34] Z. Hu, L. Wang, K. Zhang, J. Wang, F. Cheng, Z. Tao, J. Chen, MoS_2 nanoflowers with expanded interlayers as high-performance anodes for sodium-ion batteries, Angew. Chem. Int. Ed. 53 (2014) 12794–12798.
[35] Z.H. Ping, Q.T. Nguyen, S.M. Chen, J.Q. Zhou, Y.D. Ding, States of water in different hydrophilic polymers - DSC and FTIR studies, Polymer 42 (2001) 8461–8467.
[36] D. Dolar, N. Drasinac, K. Kosutic, I. Skoric, D. Asperger, Adsorption of hydrophilic and hydrophobic pharmaceuticals on RO/NF membranes: identification of interactions using FTIR, J. Appl. Polym. Sci. 134 (2017) 44426.
[37] M. Al-Shammiri, Evaporation rate as a function of water salinity, Desalination 150 (2002) 189–203.